RevMexAA (Serie de Conferencias), **9**, 40–47 (2000)

X-RAY LINE SPECTROSCOPY OF MASSIVE X-RAY BINARIES

D. A. Liedahl,[1] M. Sako,[2] P. S. Wojdowski,[1] F. Paerels,[2] and S. M. Kahn[2]

RESUMEN

Los espectros de *ASCA* dan una imagen detallada de las propiedades espectrales en rayos-X de los vientos estelares en binarias de rayos-X. Usando modelos atómicos con detalles de las cascadas de recombinación, hemos re-examinado los datos de archivo de Vela X-1 y Cen X-3 con modelos simples para la geometría y la distribución de velocidades del viento. Nuestro enfoque se centra en la distribución de medidas de emisión diferenciales *aparentes* (DEM) y sus dependencias en la fase orbital y parámetros del viento. Los espectros modelados se generan con una malla de distribuciones teóricas del DEM. Tenemos buenos ajustes y obtenemos restricciones a los parámetros de los vientos. Presentamos un resumen del método y mostramos que, aún cuando las estrellas compañeras de Vela X-1 y Cen X-3 tienen pérdidas de masa comparables, los vientos de estos dos sistemas tienen diferencias muy importantes.

ABSTRACT

Spectra from *ASCA* have provided the most detailed view to date of the X-ray spectral properties of stellar winds in massive X-ray binaries. Using detailed atomic models that account for recombination cascade kinetics, we have re-examined archival data from Vela X-1 and Cen X-3 in the context of simple models of their wind geometries and velocity distributions. Our approach emphasizes *apparent* differential emission measure (DEM) distributions, and their dependence on orbital phase and wind parameters. A grid of theoretical DEM distributions is used to generate model spectra, which are compared to the data. We obtain good fits, and derive constraints on the stellar wind parameters. We provide a summary of the method, and show that, even though the companion stars in Vela X-1 and Cen X-3 have comparable mass-loss rates, the winds in these two systems are dramatically different in character.

Key Words: **PULSARS: INDIVIDUAL (CEN X-3, VELA X-1) — STARS: MASS-LOSS — STARS: WINDS, OUTFLOWS — X-RAYS: GENERAL**

1. INTRODUCTION

Massive X-ray binaries (MXRBs) consist of a high-mass ($\sim 10\ M_\odot$ or more) star and a close compact object, usually a neutron star, but sometimes a black hole (e.g., Cyg X-1). The high-mass stellar companions in MXRBs belong to the classes O, B, or Be, and generate UV-driven supersonic winds with mass-loss rates $\sim 10^{-7}$–$10^{-6}\ M_\odot\ \mathrm{yr}^{-1}$. Although the total system luminosity in MXRBs is usually dominated by the UV radiation from the companion, MXRBs make themselves conspicuous by their X-ray luminosities, which are typically $L_\mathrm{x} \sim 10^{36}$ erg s^{-1}. Many of these objects contain spinning neutron stars with high magnetic fields, giving rise to the X-ray pulsar phenomenon. Analyses of the pulse arrival times in X-ray pulsars have allowed precise determinations of the system parameters for several MXRBs (for a review, see White, Nagase, & Parmar 1995).

[1]Physics Department, Lawrence Livermore National Laboratory, USA
[2]Columbia Astrophysics Laboratory and Department of Physics, Columbia University, USA

As the compact object in a MXRB intercepts the stellar wind, it captures some of the wind gravitationally. The subsequent accretion of material onto the compact object powers the X-ray luminosity (Davidson & Ostriker 1973). MXRBs with X-ray luminosities of $\sim 10^{36}$ erg s^{-1} fall into a sub-category in which accretion from the wind appears to account for $L_{\rm x}$ (White 1985). In other cases the X-ray luminosity exceeds by far what one would predict based on the system parameters and estimates of $\dot{M}$. Examples are Cen X-3 ($L_{\rm x} \sim 10^{38}$ erg s^{-1}) and SMC X-1, with $L_{\rm x} \sim 5 \times 10^{38}$ erg s^{-1} (White, Swank, & Holt 1983). In these systems, an accretion disk efficiently mediates the transfer of material to the neutron star, although a substantial stellar wind is also present (cf. Day & Stevens 1993). In either case, the X-ray source plays a role in modifying the physical conditions in the wind (Hatchett & McCray 1977), which is the focus of this article.

The research presented here has been largely motivated by *ASCA* spectra from three MXRBs, Vela X-1, Cen X-3, and Cyg X-3. The spectrum of Vela X-1 obtained during eclipse of the neutron star by its B supergiant companion showed unequivocally that the X-ray spectrum of the wind is dominated by line emission (Nagase et al. 1994). Ebisawa et al. (1996) used the orbital phase variations of the Cen X-3 spectrum to infer the size of the ionization zones of highly-ionized iron. The high quality of the Cyg X-3 spectrum (Kitamoto et al. 1994) enabled measurements of electron temperatures in three ionization zones, using fits to radiative recombination continua of hydrogen-like magnesium, silicon, and sulfur (Liedahl & Paerels 1996). Our group has re-examined spectra from Vela X-1 (Sako et al. 1999) and Cen X-3 (P. S. Wojdowski, D. A. Liedahl, & M. Sako 2000, in preparation) in the context of global geometrical models of these systems, found that good fits can be obtained, and found that constraints on the wind structure can be derived. This article includes a description of the methodology and a summary of the results.

2. IONIZATION IN AN X-RAY IRRADIATED WIND

The charge state distribution and temperature in a wind that is optically thin to the ionizing X-ray continuum are characterized by the ionization parameter $\xi = L/nr^2$ (Tarter, Tucker, & Salpeter 1969), where r is the distance of a wind parcel from the point source of X rays, and n is the number density. To evaluate this in the context of a theoretical geometrical model of a MXRB, we need an expression for the density. Denote by R the distance as measured from the companion's center. In a spherically symmetric wind, the mass continuity equation can be used to express the local density in terms of the local wind velocity and the mass-loss rate

$$n(R) = \frac{\dot{M}}{4\pi\mu m_p R^2 v(R)}, \tag{1}$$

where μ is the mean atomic weight, and $m_{\rm p}$ is the proton mass. The velocity profile is usually approximated by

$$v(R) = v_\infty \left(1 - \frac{R_*}{R}\right)^\beta, \tag{2}$$

where v_∞ is the terminal velocity, and is typically $\sim 10^8$ cm s^{-1}. The parameter $\beta \approx 0.8$ (Friend & Abbott 1986; Pauldrach, Puls, & Kudritzki 1986), a modification of the profile first derived by Castor, Abbott, & Klein (1975), where $\beta = 0.5$, appropriate in the limit of a pointlike UV source. Then using equations (1) and (2), ξ is given as

$$\xi = 4\pi\mu m_{\rm p} v_\infty \, \frac{L_{\rm x}}{\dot{M}} \left(\frac{R}{r}\right)^2 \left(1 - \frac{R_*}{R}\right)^\beta. \tag{3}$$

If we orient a spherical coordinate system centered on the companion, such that the polar angle θ is defined relative to the line of centers, then the quantities r and R are related by $(r/R)^2 = 1 + (a/R)^2 - 2(a/R)\cos\theta$, where a is the binary separation. The spatially independent part of equation (3) ($4\pi\mu m_{\rm p} v_\infty L_{\rm x}/\dot{M}$) has the dimensions of an ionization parameter, and provides a characteristic value of ξ for a particular system. Note also that this is the value of ξ that the wind approaches as $R \to \infty$.

For a location fixed in the co-rotating frame, the ratio $L_{\rm x}/\dot{M}$ in equation (3) expresses the competition between ionization and recombination. Increasing $L_{\rm x}$ with $\dot{M}$ fixed increases the photoionization rate, which increases ξ, while increasing $\dot{M}$ with $L_{\rm x}$ fixed increases the recombination rate, which decreases ξ. (In the simplest picture, with a steady-state, spherically symmetric, smooth wind, $L_{\rm x}$ and $\dot{M}$ are not allowed to vary

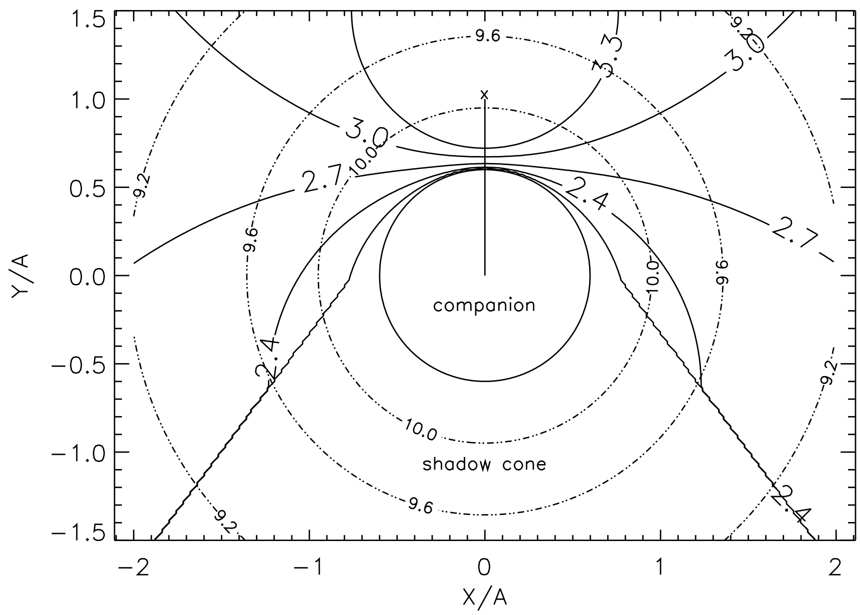

Fig. 1. Ionization and density contours for a spherically symmetric homogeneous wind for system parameters $L_{\rm x} = 4\times10^{36}$ erg s^{-1}, $\dot{M} = 5\times10^{-7} M_\odot$ yr^{-1}, $v_\infty = 2000$ km s^{-1}, $\beta = 0.5$, companion star radius $R_* = 6\times10^{11}$ cm (heavy circle), binary separation $a = 10^{12}$ cm, indicated by the vertical line connecting the companion center to the X-ray source (line of centers). Coordinate system is centered on the companion star, and the axes are labeled in multiples of a. Contours of constant $\log\xi$ are shown as solid lines with the larger numerical labels. Three surfaces (9.2, 9.6, and 10.0) of constant $\log n$ (cm^{-3}) are shown as dotted lines with the smaller numerical labels. Diagonal lines delineate the shadow cone. The line of centers defines an axis of cylindrical symmetry.

Astrophysical Plasmas: Codes, Models, and Observations (Mexico City, 25-29 October 1999)
Editors: Jane Arthur, Nancy Brickhouse, & José Franco

independently, since $L_{\rm x} \propto \dot{M}$.) Here, however, we are more interested in the geometrical distribution of ξ, assuming that $L_{\rm x}$ and $\dot{M}$ are fixed.

Hatchett & McCray (1977) show that surfaces of constant ξ for a constant velocity wind in a MXRB define a bispherical geometry, in which two sets of non-concentric spheres surround the companion and the X-ray source, respectively. They also show that for a velocity law given by the CAK formalism (Castor et al. 1975), i.e., equation (2) with $\beta = 0.5$, a similar, though not precisely bispherical, geometry is obtained. An example of "iso-ξ" contours for $\beta = 0.5$ is shown in Figure 1. Since, according to photoionization models, the electron temperature is a function of ξ, the ξ contours are also isothermal surfaces. The parameters chosen for this calculation are representative of the wind-fed MXRBs, such as Vela X-1. Since the ionization timescale and recombination timescale (e.g., $T_{\rm rec} \sim 10^{11}$ s cm$^{-3}/n$) are virtually instantaneous with respect to the orbital period, this structure can be considered as fixed in the co-rotating frame, if there is no intrinsic time dependence. The X-ray pulsar may, however, change the local ionization balance in a periodic manner. We ignore this subtlety for now (cf. Kallman, McCray, & Voit 1987).

3. DIFFERENTIAL EMISSION MEASURE IN PHOTOIONIZED GAS

For an emission line connecting an upper energy level u to a lower energy level l in charge state i of element z we define a *recombination line power* $P_{\rm ul}$ (c.g.s. dimensions erg cm^3 s^{-1}) in terms of the line emissivity $j_{\rm ul}$, according to $j_{\rm ul} = n_{\rm e}^2 P_{\rm ul}$. In terms of the elemental abundance $A_{\rm z}$ and the charge state fraction of the recombining ion $f_{\rm i+1}$, the line power has the explicit form

$$P_{\rm ul} = A_{\rm z}\,\frac{n_{\rm H}}{n_{\rm e}}\,f_{\rm i+1}\alpha_{\rm i+1}\,\eta_{\rm ul}\,E_{\rm ul}\quad, \tag{4}$$

where α_{i+1} is the total recombination rate $(i+1 \rightarrow i)$, η_{ul} is the fraction of recombinations leading to emission of the line $u \rightarrow l$, and E_{ul} is the line energy. For each line, we calculate the quantity η_{ul} by solving the rate equations for the level population distributions of charge state i, assuming that only the ground state of charge state $i+1$ is populated. This is probably a valid assumption in stellar wind sources, for which the densities of the X-ray emission-line regions are $\sim 10^{10}$ cm^{-3}. The rate equations are solved for a range of temperatures up to ~ 100 eV, and the quantities $\alpha_{i+1}\ \eta_{ul}$ are fit to power-laws, i.e., $\alpha_{i+1}\ \eta_{ul} = C_{ul} T^{-\gamma_{ul}}$.

Our current spectral models include H-like and He-like ions of C, N, O, Ne, Mg, Si, S, Ar, Ca, and Fe, as well as L-shell Fe (Liedahl & Paerels 1996). The line powers for Fe L-shell ions include contributions from cascade following $\Delta n = 0$ dielectronic recombination (Liedahl 1999). The models consist of ten shells (i.e., $n = 1-10$), where the tenth is a "superlevel," a level with an enhanced statistical weight to account for recombinations into shells with $n \geq 10$. The models also include radiative recombination continua (RRC), with rate coefficients calculated consistently with those of the recombination lines.

Recombination lines can be associated with particular values of ξ—each line can be assigned a "ξ of formation" ξ_f. These occur at the value of ξ for which $P_{ul}(\xi)$ is a maximum, equivalent to maximizing $f_{i+1}(\xi)\alpha_{i+1}[T(\xi)]$, where the XSTAR photoionization code (Kallman & Krolik 1994) is used to find $f_{i+1}(\xi)$ for each ion in our spectral model. It is thus natural to plot the apparent emission measure vs. ξ (Sako et al. 1999), with each charge state for which spectroscopic data exist represented by a point, assuming that $L_{ul} = EM_{i+1}(\xi_f)P_{ul}(\xi_f)$, where EM_{i+1} denotes the emission measure of the recombining ion at a particular value of ξ. It is well-known, however, that recombination emission, especially from hydrogenic ions, is efficient over a wide range in ξ (Hirano et al. 1987; Ebisawa et al. 1996). Therefore, constructing an empirical DEM distribution in this way leaves us with, at best, a crude approximation of the true, continuous DEM distribution.

With a geometrical model of the system, we can improve upon this situation. One can generate a theoretical DEM distribution by dividing the three-dimensional space into small volume elements (ΔV), calculate $n_e^2 \Delta V$ from equations (1) and (2), and add the result to the appropriate ξ-bin, as determined from equation (3). This is straightforward using the MXRB model described in the previous section. Note that the theoretical DEM distribution is fully determined by L_x, $\dot{M}$, v_∞, β, a, and R_*, provided that the occultation of part of the X-ray emission-line region by the companion is accounted for. Actually, the parameterization is simpler, since $\dot{M}$ and v_∞ appear in the equations as $\dot{M}/v_\infty$, and L_x, a, and R_* are sometimes known independently. Thus for Vela X-1, the DEM distribution can be parameterized by $\dot{M}$ and β, since there is also an independent measurement of v_∞ (Dupree et al. 1980).

The line luminosity for the transition $u \rightarrow l$ is the integral over ξ of the line power weighted by the DEM distribution,

$$L_{ul} = \int d\xi\ \frac{d(EM_{i+1})}{d\xi}\ P_{ul}(\xi), \tag{5}$$

with an analogous expression for the RRC monochromatic luminosity. Therefore, the spectrum of the reprocessing material is also fully determined by the parameters given above. By generating theoretical spectra on the parameter grid, then comparing with spectroscopic data, the parameters themselves can be determined if an acceptable fit can be found.

While the production of fluorescence K line radiation is not normally thought of as a two-body process ($L_K \propto Ln$ in the limit that the fluorescing medium is optically thin to the ionizing radiation), it can be treated as such by recasting the previous proportionality as $L_K \propto n^2\xi$, using the definition of ξ. Thus the fluorescence lines can, in principle, be used to extend the DEM distribution to lower values of ξ (Wojdowski, Clark, & Kallman 2000). To do so, however, requires that we can decompose the fluorescent features into their respective charge states, so that ξ itself can be specified. Limited by the energy resolution of the current data, it is possible only to impose an upper limit to ξ for each fluorescence line complex.

4. VELA X-1 AND CEN X-3

Remarkably, the simple approach outlined above results in excellent fits to the eclipse spectra of Vela X-1 and Cen X-3, as shown in Figure 2. The corresponding DEM distributions are shown in Figure 3. For Vela X-1, we fit the eclipse spectrum by two methods. First, we dispensed with the global model of the source, and used a multi-component model in XSPEC, with the normalization of each ion as a fitting parameter. A satisfactory χ^2 was found, leading to an empirical DEM distribution (Sako et al. 1999). Second, with only $\dot{M}$ and β as

Astrophysical Plasmas: Codes, Models, and Observations (Mexico City, 25-29 October 1999)
Editors: Jane Arthur, Nancy Brickhouse, & José Franco

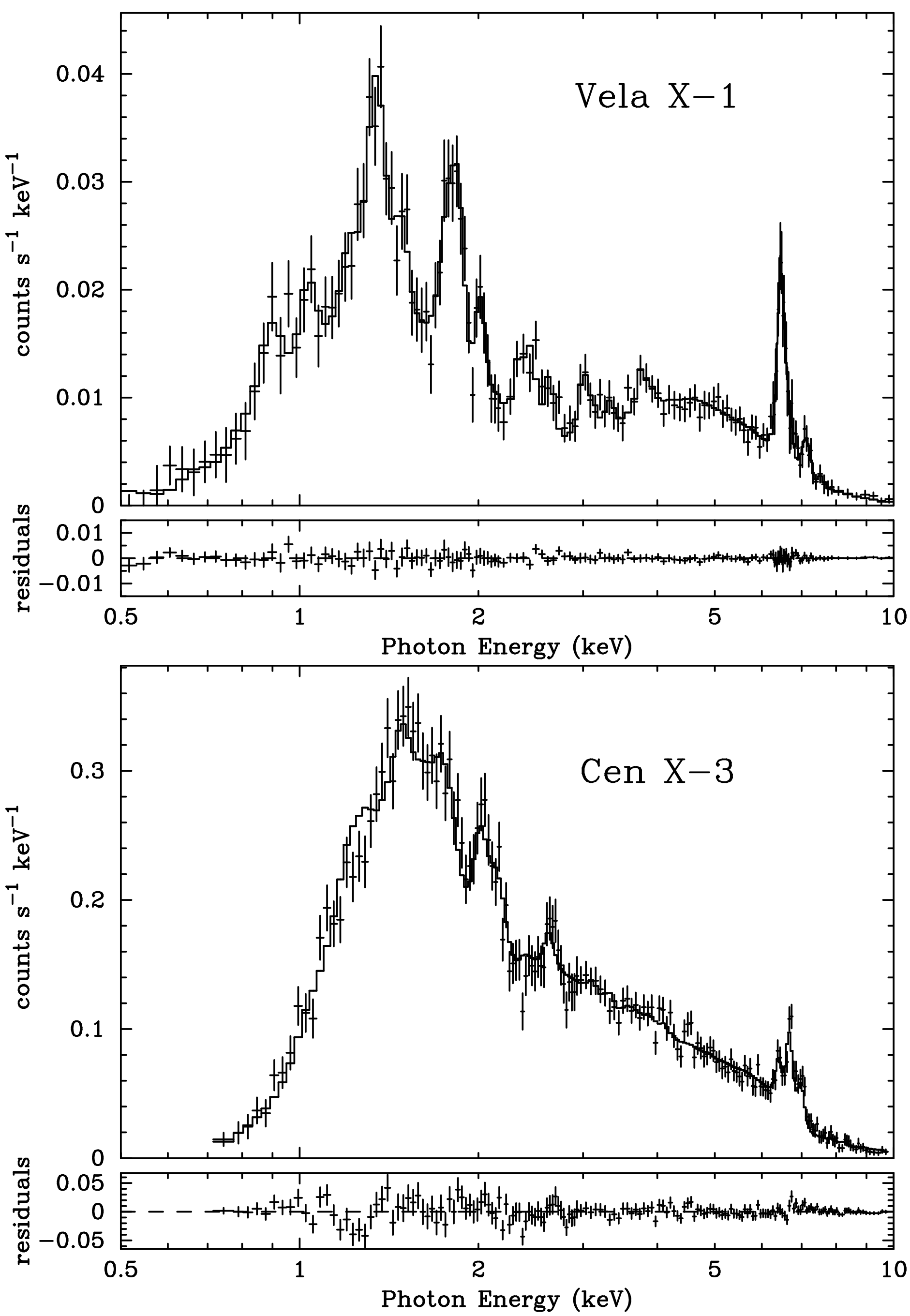

Fig. 2. Best fit models compared to eclipse spectra of Vela X-1 (*top*; Sako et al. 1999) and Cen X-3 (*bottom*; P. S. Wojdowski, D. A. Liedahl, & M. Sako, in preparation). Residuals (*data* - *model*) are also shown, in the same units.

fitting parameters, a grid of model spectra was generated, then compared with the data, resulting in a χ^2 surface over the 3500-point (50 × 70) grid. This procedure yielded tight constraints on $\dot{M}$ and β, with best-fit values $\dot{M} = 2.7 \times 10^{-7}\ M_\odot\ \mathrm{yr}^{-1}$ and $\beta = 0.79$. For Cen X-3, spectra from four orbital phase intervals were fit simultaneously, using spectral models parameterized by $\dot{M}/v_\infty$ and β (there is currently no independent measurement of v_∞ for this source). We find that, $\dot{M}/v_\infty = 1.4 \times 10^{-6}\ v_{1000}^{-1}\ M_\odot\ \mathrm{yr}^{-1}$, and $\beta = 0.57$, where v_{1000} is the terminal velocity expressed as a multiple of 1000 km s^{-1}. Only the eclipse spectrum and the best fit model are shown in Figure 2.

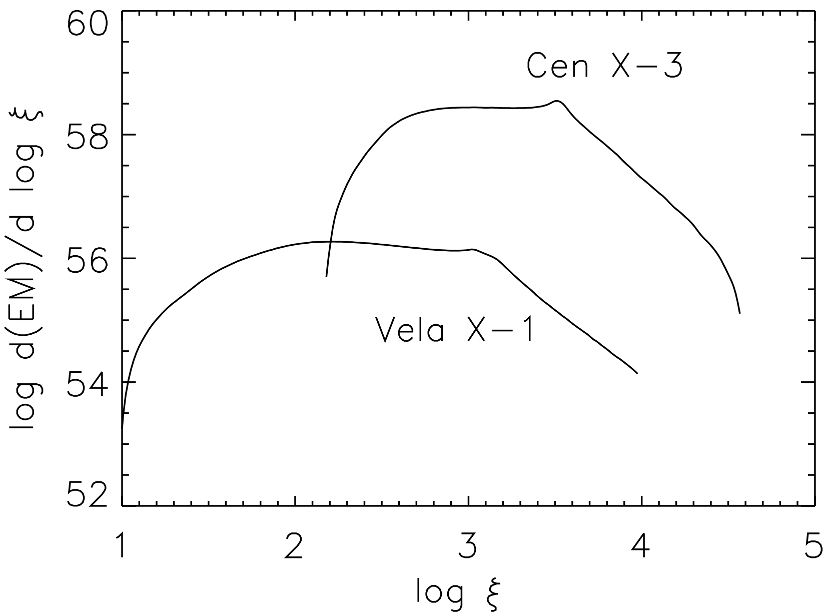

Fig. 3. Comparison of differential emission measure distributions for Vela X-1 and Cen X-3. For Vela X-1, the contribution from low-ξ fluorescing material, which would cause an upturn in the DEM curve moving to lower ξ, is not included. The small bump in each curve corresponds to the DEM near the system midplane. The huge difference in the integrated emission measures for $\log \xi > 1.5$ is a consequence of the wind inhomogeneity in Vela X-1.

Astrophysical Plasmas: Codes, Models, and Observations (Mexico City, 25-29 October 1999)
Editors: Jane Arthur, Nancy Brickhouse, & José Franco

For Vela X-1, while our derived β is in accord with theoretical expectations (Friend & Abbott 1986; Pauldrach et al. 1986), $\dot{M}$ is anywhere from 3–10 times smaller than literature values. This apparent discrepancy is magnified by the failure of the global model to account for the fluorescent line emission and the absorbing column density, both of which require substantial column densities ($\sim 10^{22}$ cm^{-2}) of near-neutral ions. We have concluded that the problem lies not in the analysis of the recombination lines, for which $\log \xi > 1.5$, but in our inability to properly fit the fluorescence lines, produced at lower ξ, into the DEM framework. If we superimpose a population of clouds with densities $\sim 10^{11}$ cm^{-3} (to maintain a low value of ξ) and sizes $\sim 10^{11}$ cm (see below), and suppose that this cloud population subtends a solid angle at the neutron star of 4π, then we arrive at a mass-loss rate $\dot{M} \sim 3 \times 10^{-6}\ M_\odot\ \mathrm{yr}^{-1}$, in much better agreement with previously derived values. Now, however, about 90% of the wind mass is in the form of clumps. Note that this does not force us to alter our quantitative results regarding the highly-ionized wind component, since about 95% of the wind volume is in the form of this more highly-ionized gas, i.e., *geometrically*, the clumps constitute a small perturbation to the model. This inhomogeneous wind model accounts for the X-ray spectrum (recombination lines, fluorescence lines, scattered continuum), the near-neutral column density, and provides material with relatively low ionization levels that has a large covering fraction with respect to the companion, needed for consistency with the observed P Cygni profiles in the UV band (Dupree et al. 1980).

Line-driven stellar winds are subject to several instabilities (MacGregor, Hartmann, & Raymond 1979; Lucy & White 1980; Owocki & Rybicki 1984), such as the Rayleigh-Taylor instability, which will produce clumps with sizes $\sim 10^{11}$ cm (Carlberg 1980). Thus it is not entirely surprising that we should find a need to invoke an inhomogeneous wind to explain the X-ray spectra. On observational grounds, clumpiness has already been suggested as a way to explain the absorption behavior in the MXRBs Vela X-1 (Nagase et al. 1986) and 4U 1700-37 (White, Kallman, & Swank 1983). Our approach has led to a more quantitative model of the clumped wind, and shows that, at least for Vela X-1, a clumped wind is probably typical. Still, while the characteristics of the clumps in our model are reasonable, they are more or less *ad hoc*, and do not accommodate a cloud population that is likely to possess a distribution of sizes and densities.

For Cen X-3, by contrast, we already know that any clump population should have a negligible effect on the X-ray spectrum, as evidenced by the near constancy with orbital phase of the equivalent width of the fluorescent Fe K complex (Ebisawa et al. 1996). In other words, were the wind highly clumped and extended, a dramatic increase in the Fe K equivalent width would accompany eclipse of the compact X-ray source. Vela X-1, for example, *does* show a large-amplitude variability in the Fe K equivalent width (Sato et al. 1986). Therefore, we assume that the wind in Cen X-3 is smooth, and, for a given v_∞, assume that the best-fit $\dot{M}$ is the total mass-loss rate of the companion.

Although the two systems have similar mass-loss rates, the DEM distributions (Fig. 3) for X-ray-emitting gas are drastically different. The relatively small DEM magnitudes in Vela X-1 reflect the fact that most of the wind mass is "locked up" in dense clumps. The fact that the total emission measures (the integral of the DEM distribution) appear to be so different is not real, and simply reflects the omission of the DEM distribution for the lower-ξ region. Plotting the distribution for $\log \xi < 1.5$ would, however, require a thorough analysis of the line complexes from fluorescing material, as discussed in §3.

5. DISCUSSION

For the Vela X-1 analysis, although many of our results are only semi-quantitative, the overall model succeeds in accounting for several observational aspects of the source (Sako et al. 1999). As pointed out by D. Cohen (priv. comm.), the clumped component in Vela X-1 *is the wind*; the highly-ionized component, from which we observe X-ray recombination lines, though not constituting the wind proper, appears to be serving as a proxy for the wind dynamics. This is an unexpected result. Studies of the effects of X rays on the wind-driving mechanism have shown that the radiative force decreases as wind material becomes increasingly ionized by the X-ray source (MacGregor & Vitello 1982; Stevens & Kallman 1990). Our finding that the highly-ionized wind in Vela X-1 follows a CAK-like profile thus would appear to stand in contradiction. We can only speculate at this point, but it may be that the highly-ionized wind component is material that has evaporated from clumps exposed to the X-ray source, and is consequently tied to the clump velocity distribution, which is driven by the conventional UV line force. Alternatively, since the clump covering fraction with respect to the companion is near unity, the ram pressure of the clumps may be pushing the more tenuous gas away from the companion, again resulting in a CAK-like profile. Finally, these two alternatives may not, in fact, be mutually exclusive, but could constitute two aspects of a larger overall picture that describes clump formation and evolution.

The case of Cen X-3 is even more surprising, since its wind is more highly ionized than that of Vela X-1. We have ruled out reprocessing in a disk wind, owing to the absence of sufficient orbital variation in the line fluxes. Day & Stevens (1993) have suggested that a thermally-driven wind is being blown from the X-ray illuminated face of the companion, which may help to explain the high accretion rate onto the neutron star ($L_{\rm x} \sim 10^{38}$ erg s^{-1}). However, it seems likely that such a wind will be concentrated along the line of centers, which, again, suggests a more pronounced orbital modulation of the reprocessed line flux than what is observed. It is easy to suggest that the lack of clumpiness in the Cen X-3 wind is related to its very high X-ray luminosity, but we have yet to address this issue in detail. Clearly, these matters require further investigation.

It is well known that stellar winds in MXRBs are not spherically symmetric. Nevertheless, we obtain good fits to *ASCA* spectra under that assumption. Our models make very definite predictions regarding line profiles and their dependence upon orbital phase. We hope to test these predictions and begin to add refinements to our simple models when data of higher spectral resolution become available. A more satisfactory empirical description of the wind physics awaits spectroscopic data that allow (1) identifications of the individual charge states that compose the fluorescence "features," (2) measurements of Doppler shifts in emission lines, and (3) measurements of line broadening, the latter two both at the few $\times$ 100 km s^{-1} level. Some of these goals may be achieved with the new X-ray observatories—*Chandra*, *XMM*, and *Astro-E*—and can be easily attained with an observatory on a par with *Constellation-X*.

D. A. L. and P. S. W. were supported in part by the NASA Long Term Space Astrophysics Program grant S-92654-F. S. M. K., F. P., and M. S. were supported by the NASA Long Term Space Astrophysics Program grant NAG5-3541. Work at LLNL was performed under the auspices of the U. S. Department of Energy, Contract No. W-7405-Eng-48.

REFERENCES

Carlberg, R. G. 1980, ApJ, 241, 1131
Castor, J. I., Abbott, D. C., & Klein, R. I. 1975, ApJ, 195, 157
Davidson, K., & Ostriker, J. P. 1973, ApJ, 179, 585
Day, C. S. R., & Stevens, I. R. 1993, ApJ, 403, 322
Dupree, A. K., et al. 1980, ApJ, 238, 969
Ebisawa, K., et al. 1996, PASJ, 48, 425
Friend, D. B., & Abbott, D. C. 1986, ApJ, 311, 701
Hatchett, S., & McCray, R. 1977, ApJ, 211, 552
Hirano, T., Hayakawa, S., Nagase, F., Masai, K., & Mitsuda, K. 1987, PASJ, 39, 619
Kallman, T. R., & Krolik, J. H. 1994, XSTAR–A Spectral Analysis Tool, HEASARC (Greenbelt: NASA/GSFC)
Kallman, T. R., McCray, R., & Voit, G. M. 1987, ApJ, 317, 746
Kitamoto, S., Kawashima, K., Negoro, H., Miyamoto, S., White, N. E., & Nagase, F. 1994, PASJ, 46, L105
Liedahl, D. A. 1999, in Lecture Notes in Physics 520, X-Ray Spectroscopy in Astrophysics, ed. J. van Paradijs & J. Bleeker (Amsterdam: Springer), 189
Liedahl, D. A., & Paerels, F. 1996, ApJ, 468, L33
Lucy, L. B., & White, R. L. 1980, ApJ, 241, 300
MacGregor, K. B., Hartmann, L., & Raymond, J. C. 1979, ApJ, 231, 514
MacGregor, K. B., & Vitello, P. A. 1982, ApJ, 259, 267
Nagase, F., Hayakawa, S., Sato, N., Masai, K., & Inoue, H. 1986, PASJ, 38, 547
Nagase, F., Zylstra, G., Sonobe, T., Kotani, T., & Inoue, H. 1994, ApJ, 436, L1
Owocki, S. P., & Rybicki, G. B. 1984, ApJ, 284, 337
Pauldrach, A., Puls, J., & Kudritzki, R. P. 1986, A&A, 164, 86
Sako, M., Liedahl, D. A., Paerels, F., & Kahn, S. M. 1999, ApJ, 525, 921
Sato, N., et al. 1986, PASJ, 38, 731
Stevens, I. R., & Kallman, T. R. 1990, ApJ, 365, 321
Tarter, C.B., Tucker, W. H., & Salpeter, E. E. 1969, ApJ, 156, 943
White, N. E. 1985, in Interacting Binaries, ed. P. Eggleton & J. Pringle (Dordrecht: Reidel), 249
White, N. E., Kallman, T. R., & Swank, J. H. 1983, ApJ, 269, 264
White, N. E., Nagase, F., & Parmar, A. N. 1995, in X-ray Binaries, ed. W. Lewin, J. van Paradijs, & E. van den Heuvel (Cambridge: Cambridge University Press), 1
White, N. E., Swank, J. H., & Holt, S. S. 1983, ApJ, 270, 711
Wojdowski, P. S., Clark, G. W., & Kallman, T. R. 2000, ApJ, in press

D. A. Liedahl and P. S. Wojdowski: Physics Department, Lawrence Livermore National Laboratory, 7000 East Avenue, Livermore, CA 94550, USA (duane, patrickw@virgo.llnl.gov).
S. M. Kahn, F. Paerels and M. Sako: Columbia Astrophysics Laboratory and Department of Physics, Columbia University, 538 West 120th Street, New York, NY 10027, USA (skahn, frits, masao@astro.columbia.edu).